

Anchoring effects at the isotropic-nematic interface in liquid crystals

R. L. C. Vink

*Institut für Theoretische Physik II, Heinrich Heine Universität Düsseldorf,
Universitätsstraße 1, 40225 Düsseldorf, Germany*

(Dated: November 15, 2018)

The isotropic-to-nematic transition in liquid crystals is studied in $d = 3$ spatial dimensions. A simulation method is proposed to measure the angle dependent interfacial tension $\gamma(\theta)$, with θ the anchoring angle of the nematic phase at the interface. In addition, an alternative liquid crystal model is introduced, defined on a lattice. The advantage of the lattice model is that accurate simulations of anchoring effects become possible. For the lattice model, $\gamma(\theta)$ depends sensitively on the nearest-neighbor pair interaction, and both stable and metastable anchoring angles can be detected. We also measure $\gamma(\theta)$ for an *off-lattice* fluid of soft rods. For soft rods, only one stable anchoring angle is found, corresponding to homogeneous alignment of the nematic director in the plane of the interface. This finding is in agreement with most theoretical predictions obtained for hard rods.

PACS numbers: 83.80.Xz, 68.05.-n, 68.03.Cd, 64.70.Md, 61.30.Hn

I. INTRODUCTION

A fluid consisting of elongated molecules is more difficult to describe than one in which the molecules are simply spherical. In the case of elongated molecules, there are not only translational degrees of freedom, but also orientational ones. This additional complexity gives rise to many interesting effects, not found in spheres. For example, infinitely slender rods in three dimensions undergo a first-order phase transition from an isotropic to a nematic phase, provided the density is sufficiently high [1]. Both the isotropic and the nematic phase lack translational order, but in the nematic phase the rods have aligned, giving rise to long-range orientational order.

The orientation of the nematic phase is an important quantity. In applications involving nematics at walls, the angle of the nematic director at the wall is often crucial. This angle is called the tilt or anchoring angle. Typically, there is a preferred tilt angle the nematic phase will assume, but the precise value depends sensitively on factors such as surface chemistry, particle shape, and temperature [2, 3, 4]. Similarly, anchoring effects also occur at the isotropic-to-nematic (IN) transition. The first-order nature of that transition implies phase coexistence, whereby isotropic domains coexist with nematic domains, separated by interfaces. As Fig. 1 shows, the

orientation of the nematic phase with respect to the interface becomes an additional parameter. In Fig. 1(a), the nematic director points in the plane of the interface, which is called planar or homogeneous alignment. In Fig. 1(b), the director is perpendicular to the interface, which is known as homeotropic alignment.

From symmetry considerations alone, it is clear that homogeneous and homeotropic anchoring are different. For homeotropic anchoring, there is still rotational symmetry around the interface normal; for homogeneous anchoring, no such symmetry is present. This difference is known to affect the spectrum of capillary waves. For homogeneous anchoring, the spectrum becomes anisotropic in the short wavelength limit [5, 6, 7, 8]. In contrast, for homeotropic anchoring, the spectrum remains isotropic at all wavelengths. In other words, as this example shows, the anchoring angle affects the interfacial properties qualitatively. Given a set of particle interactions, it is therefore important to be able to predict the anchoring angle. This has led to the concept of an angle dependent interfacial tension $\gamma(\theta)$, with θ the tilt or anchoring angle. Here, θ is defined as the angle between the nematic director and the plane of the IN interface. Homogeneous ($\theta = 0$) and homeotropic ($\theta = 90$) anchoring are most common, although θ could, in principle, be anywhere between 0 and 90 degrees. In theoretical investigations, the anchoring angle is given by the angle which minimizes $\gamma(\theta)$. For hard rods, this is typically $\theta = 0$, corresponding to homogeneous anchoring [9, 10, 11, 12, 13, 14], but the precise behavior is quite subtle. For example, the results of Ref. 9 also suggest that homeotropic anchoring may be metastable. In addition, for very short rods, anchoring angles between 0 and 90 degrees have also been reported [12].

Unfortunately, it remains difficult to verify these theoretical findings in a computer simulation. On the one hand, efficient simulation methodology for problems of this kind is scarce. The state-of-the-art is to extract $\gamma(\theta)$ from the anisotropy of the pressure tensor [5, 15, 16],

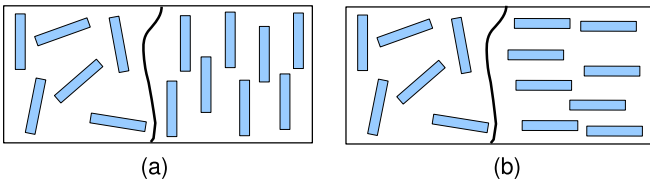


FIG. 1: Schematic representation of isotropic-nematic phase coexistence. The isotropic phase is on the left, the nematic on the right. Shown are (a) homogeneous anchoring, and (b) homeotropic anchoring.

a technique which is somewhat prone to statistical error. On the other hand, the particle interactions used in many theoretical investigations are not convenient for simulations. The hard rod potential, for instance, often used in theory, gives rise to a very small interfacial tension. In order to stabilize the IN interface, simulations of hard rods require huge system sizes, implying long equilibration times and, consequently, data with considerable statistical uncertainty.

The purpose of this paper is to improve on this state of affairs. The primary aim is to present a simulation method capable of measuring the angle dependent interfacial tension accurately. The method is presented in Section II. As it turns out, the method is general, and applies to lyotropic (density driven) systems, such as rods or platelets, as well as to thermotropic (temperature driven) lattice systems. The second aim is to introduce a new liquid crystal model, one which is easy to simulate, but which nevertheless features an IN transition with anchoring effects. The model we propose is defined on a *lattice*, and resembles the Lebwohl-Lasher (LL) model [17], but with two essential modifications. Since the model is easy to simulate, it lends itself perfectly for an investigation of anchoring effects. The liquid crystal model, and the subsequent determination of its $\gamma(\theta)$, are presented in Section III. Next, in Section IV, we determine $\gamma(\theta)$ for a fluid of soft rods. These particles are already more complicated to simulate. Nevertheless, guided by the experience obtained for the simple lattice model, a meaningful interpretation of the simulation data is possible. We end with a summary and outlook in the last section.

II. SIMULATION METHOD

In this Section, we present our method to extract the angle dependent interfacial tension $\gamma(\theta)$ in liquid crystals. The use of so-called *order parameters* is crucial for our method: suitable order parameters are therefore discussed first. Next, we show how the order parameter distribution may be used to obtain phase coexistence properties, as well as interfacial tensions, which summarizes the key ingredients of previous work [18, 19]. Finally, we show how this methodology can be modified, to also capture the angular dependence of the interfacial tension, by means of a simple constraint.

A. Order parameters

Since we are dealing with the IN transition in liquid crystals, a suitable order parameter is the nematic order parameter S , defined as the maximum eigenvalue of the orientational tensor Q , whose elements read as:

$$Q_{\alpha\beta} = \frac{1}{2N} \sum_{i=1}^N (3d_{i\alpha}d_{i\beta} - \delta_{\alpha\beta}). \quad (1)$$

Here, $d_{i\alpha}$ is the α component ($\alpha = x, y, z$) of the orientation \vec{d}_i of molecule i (normalized to unity), $\delta_{\alpha\beta}$ is the Kronecker delta, and N the number of molecules. Note that S is invariant under the inversion $\vec{d}_i \rightarrow -\vec{d}_i$ of single molecules, which is the characteristic symmetry of liquid crystals, and also that S does not depend on the center of mass coordinates. In the isotropic phase, S is close to zero. In the nematic phase, where the molecules have aligned, S is close to unity. Another important quantity is the (normalized) eigenvector $\vec{n} = (n_x, n_y, n_z)$ associated with S . The vector \vec{n} is called the director, and it corresponds to the overall preferred direction of the molecular orientations in the nematic phase. Again, the directions $\vec{n} \rightarrow -\vec{n}$ are equivalent: the convention in this work is to pick the vector with $n_z > 0$.

The nematic order parameter, being zero in the isotropic phase and (close to) unity in the nematic phase, is a convenient quantity to detect the IN transition in liquid crystals. However, different quantities may be used as well. For example, in thermotropic (temperature driven) liquid crystals, there is also an energy difference between the isotropic (high energy) and nematic (low energy) phase. Therefore, in thermotropic systems, energy may also be used as order parameter. Similarly, in lyotropic (density driven) liquid crystals, such as studied by Onsager [1], there is also a density difference between the isotropic (low density) and nematic (high density) phase. Therefore, in lyotropic systems, density is also a valid order parameter.

B. Order parameter distributions

Our method to obtain $\gamma(\theta)$ is based on the order parameter distribution $P(X)$, defined as the probability to observe the order parameter X during the simulation. For liquid crystals, suitable choices for X were given above. As is well known, at a first-order phase transition, the distribution $P(X)$ becomes double-peaked (bimodal). An example is provided in Fig. 2(a), which shows the energy distribution $P(E)$ of a thermotropic liquid crystal (details are provided in Section III). In thermotropic systems, $P(E)$ becomes bimodal at the transition temperature. The precise value is determined using the “equal-area” rule [20], whereby the temperature is tuned such that the area under both peaks is equal. Of course, in a lyotropic system, one would need to tune the chemical potential.

From the bimodal energy distribution of Fig. 2(a), bulk properties can readily be extracted. The peak at high energy, for example, yields the energy density of the isotropic phase; the peak at low energy of the nematic phase. Even more information is contained in the logarithm $W = \ln P(X)$, see Fig. 2(b). Note that W corresponds to *minus* the free energy of the system. We now observe a distinct flat region between the peaks. The origin of this flat region can be understood from simulation snapshots, shown schematically in Fig. 3. When the

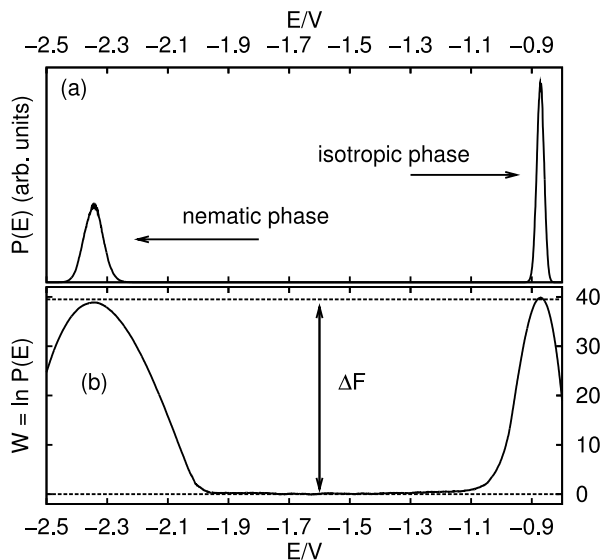


FIG. 2: (a) Coexistence distribution $P(E)$ of a thermotropic liquid crystal, interacting via Eq.(4) with $p = 10$ and $\nu = 0.5$, at the transition (inverse) temperature $\epsilon^* \approx 1.188$. The simulation box dimensions were $L = 15$ and $D = 40$. (b) The logarithm of the same distribution.

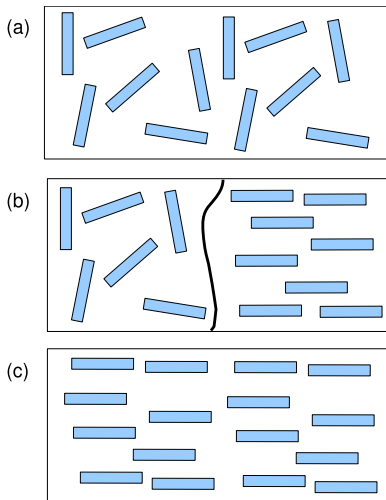


FIG. 3: Schematic simulation snapshots in (a) the bulk isotropic phase, (b) the coexistence region, and (c) the bulk nematic phase.

system is in the high-energy peak, simulation snapshots reveal a homogeneous isotropic phase (a). In the low-energy peak, snapshots reveal a homogeneous nematic phase (c). At intermediate energy, coexistence between an isotropic and nematic domain is revealed, separated by an interface (b). Note that, due to periodic boundary conditions, two such interfaces are actually present. Provided the simulation box is large enough so as to accommodate two non-interacting interfaces, the order parameter can be varied (over a limited range) with no cost

in the free energy at all, and hence a flat region in W .

The presence of a flat region in W naturally allows for an estimate of the interfacial tension [21]. In these cases, the height of the free energy barrier ΔF in Fig. 2(b) may be associated with the free energy cost of having two interfaces in the system. Since the interfacial tension is defined as the excess free energy per unit area, one simply has $\gamma = \Delta F/2A$, with A the area of one interface. It was later recognized that [22], in an elongated $L \times L \times D$ simulation box, with $D \gg L$, the interfaces form perpendicular to the elongated direction, since this minimizes the total amount of interface in the system. This leads to $A = L^2$, and consequently

$$\gamma = \Delta F/2L^2. \quad (2)$$

In previous work, the above ideas were successfully applied to the IN transition in fluids of rods [18, 19] and platelets [23]. Implementation details are also provided in these references. Of particular importance is the use of a biased sampling scheme [24], such that the simulation frequently traverses between the isotropic and the nematic phase.

C. Measuring $\gamma(\theta)$

Next, we describe how to modify the above methodology to also extract the angular dependence of the interfacial tension. We again use an elongated simulation box with periodic boundary conditions. The box is spanned by the vectors $L\hat{x}$, $L\hat{y}$, and $D\hat{z}$, with $D \gg L$. As usual, $\hat{x} = (1, 0, 0)$, $\hat{y} = (0, 1, 0)$, and $\hat{z} = (0, 0, 1)$ denote standard Cartesian unit vectors. The key additional ingredient is to add a constraint to the Hamiltonian, such that the total energy of the system becomes $E = E_0 + E_c$. Here, E_0 is the energy of the unconstrained system. For example, in a thermotropic system, E_0 could be the LL potential. In a lyotropic system, it could be the potential of hard rods. The constraint energy E_c should fulfill two criteria:

1. In the bulk isotropic and nematic phase, the influence of the constraint must vanish. In other words, E_c may not affect the bulk properties of the unconstrained system.
2. In the coexistence region, where the system schematically resembles Fig. 3(b), the director \vec{n} of the nematic phase must point along some specified tilt angle θ .

As it turns out, a suitable constraint can be written as:

$$E_c = \begin{cases} 0 & |90 - \arccos|\vec{n} \cdot \vec{z}| - \theta_t| < \delta, \\ \infty & \text{otherwise.} \end{cases} \quad (3)$$

Here, \vec{n} is the nematic director, defined in Section II A. The angles θ_t and δ are inputs of the method, and

must be specified beforehand. By using the constraint, only states whose angle between director and xy -plane is within $\theta_t \pm \delta$ are retained, while all other states are rejected.

For large systems, Eq.(3) does not affect bulk properties, since bulk properties are insensitive to the overall orientation of the phase. In contrast, in the coexistence region, the constraint has a dramatic effect. In these cases, approximately half of the simulation box is filled with an isotropic domain, and the other half with a nematic domain, see Fig. 3(b). Due to the constraint, the angle between the director of the nematic domain and the xy -plane is within $\theta_t \pm \delta$. At the same time, the use of an elongated simulation box forces the interfaces to form in the xy -plane as well. In other words, by setting θ_t , the anchoring angle θ can be fixed. More precisely, one has $\theta = \theta_t$. Naturally, the threshold angle δ should be chosen as small as possible, while, at the same time, maintaining reasonable simulational efficiency. The optimal value is model dependent, and best obtained using trial-and-error.

The idea to obtain $\gamma(\theta)$ is now clear. We first choose a tilt angle θ of interest. Next, we measure the order parameter distribution $P(X)$, in an elongated simulation box, using the methodology of Section II B. In addition, we incorporate the constraint of Eq.(3) in the simulations, using $\theta_t = \theta$. The peak positions in $P(X)$ should again yield the bulk properties of the coexisting isotropic and nematic phase. The barrier ΔF , see Fig. 2(b), can be plugged into Eq.(2) to obtain the interfacial tension at the chosen anchoring angle θ . Since bulk properties should not be affected by the constraint, we expect the peak positions in $P(X)$ to coincide with those of an unconstrained simulation. In contrast to the unconstrained simulations, a dependence of the interfacial tension on the anchoring angle θ is anticipated. To what extent these expectations are met in actual simulations will be investigated next.

III. RESULTS: LATTICE SIMULATIONS

A. Lattice model and motivation

As announced in the Introduction, we first test our method in a lattice model of a thermotropic liquid crystal. The aim is to measure $\gamma(\theta)$. The simulations are performed on a three-dimensional periodic lattice of size $V = L \times L \times D$, with $D \gg L$. To each lattice site i , a liquid crystal is attached with (normalized) orientation \vec{d}_i . The liquid crystals interact via the potential

$$E = -\epsilon \sum_{\langle i,j \rangle} \sigma_{ij} |\vec{d}_i \cdot \vec{d}_j|^p, \quad (4)$$

where the summation is over nearest neighbors, coupling constant ϵ , and exponent $p > 0$. In what follows, factors of $k_B T$ are absorbed in the coupling constant ϵ , with T

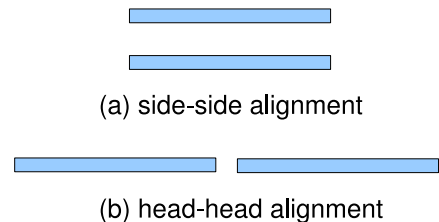


FIG. 4: Illustration of the spatial anisotropy in the liquid crystal pair interaction. In a realistic system, the energies of the above two configurations will generally differ. The LL model, however, makes no distinction.

the temperature, and k_B the Boltzmann constant. The “anisotropy” parameter is given by

$$\sigma_{ij} = 1 + \nu \left[(\vec{d}_i \cdot \vec{r}_{ij})^2 + (\vec{d}_j \cdot \vec{r}_{ij})^2 \right], \quad (5)$$

with \vec{r}_{ij} a unit vector pointing from site i to j , and ν a parameter between $-0.5 \leq \nu \leq 0.5$. On a cubical lattice, each site has six nearest neighbors. Consequently, there are only three possible axes along which the vectors \vec{r}_{ij} can be oriented.

For $p = 2$ and $\nu = 0$, this model reduces exactly to the LL model [17]. In this case, the model exhibits a first-order IN transition, but it is very weak [25]. This makes the LL model rather inconvenient for our purposes. For example, to stabilize two interfaces so as to recover the coexistence of Fig. 3(b), huge systems would be required. Such large-scale simulations are not the aim of the present work, and so we have chosen to modify the interactions appropriately. More precisely, we use a larger exponent in Eq.(4), namely $p = 10$. The effect of this is a sharper pair interaction, meaning that neighboring molecules only lower their energy when they are closely aligned. It is known that, under such interactions, first-order phase transitions become enhanced [26, 27, 28, 29, 30] (even in two dimensions).

By using $p = 10$ in Eq.(4), the model is expected to exhibit a strong first-order IN transition. Nevertheless, this is not sufficient to study anchoring because, for $\nu = 0$, the interactions are spatially isotropic. In other words, the interactions do not depend on the relative positions of the molecules, and so they cannot produce any anchoring effects at the IN interface [31]. In realistic systems, the particle interactions are typically anisotropic, see Fig. 4. Shown are two liquid crystal arrangements, labeled (a) and (b). Even though the orientations of the molecules are identical in both cases, it is clear that the energies need not be the same. In the LL model, however, for which $\nu = 0$, there is no distinction between the two arrangements. In order to nevertheless study anchoring effects, we allow $\nu \neq 0$ in Eq.(5), in which case the model does make the distinction. More precisely, we have $\sigma_{ij} = 1$ for case (a), and $\sigma_{ij} = 1 + 2\nu$ for case (b). By choosing $\nu < 0$, side-side alignment is energetically favored; choosing $\nu > 0$ favors head-head alignment. For

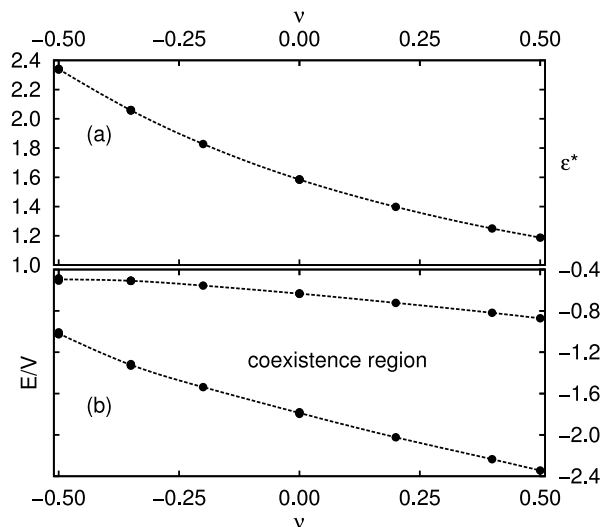


FIG. 5: Bulk properties of Eq.(4) with $p = 10$ as a function of ν . Points are actual simulation data; curves serve to guide the eye. (a) Variation of ϵ^* with ν . (b) Binodal curves, showing the energy density E/V of the isotropic phase (top curve), and of the nematic phase (lower curve), as a function of ν . At energy densities between the curves, coexistence between isotropic and nematic domains occurs; simulation snapshots will then schematically resemble Fig. 3(b).

$\nu = 0$, the interactions are isotropic, in which case no particular alignment is preferred.

B. Bulk phase behavior

We first determine the bulk behavior of Eq.(4). Recall that we keep the exponent fixed at $p = 10$. The aim is to measure the variation of the bulk properties as a function of ν . More precisely, we consider the transition inverse temperature ϵ^* , and the coexistence energy densities of the isotropic and nematic phase. To this end, we use the simulation methodology of Section II B *without* the constraint of Eq.(3). The energy distribution $P(E)$ is measured in a MC simulation, using a biased sampling scheme [24], at $\epsilon = 0$. Histogram reweighting [32] is used to determine the value of ϵ for which the “equal-area” rule is obeyed, yielding ϵ^* . The energy densities are then read-off from the peak positions. An example distribution $P(E)$ is shown in Fig. 2. The simulations are performed using single particle MC moves, whereby a random orientation is assigned to a randomly selected lattice site, accepted with the Metropolis criterion [33]. Typical lattice sizes are $L = 10 - 20$ and $D = 20 - 40$. The CPU time required to obtain $P(E)$ accurately for a large system is around 48 hours.

The variation of ϵ^* with ν is shown in Fig. 5(a). The behavior is simply monotonic: by increasing ν , ϵ^* goes down. The energy densities, shown in Fig. 5(b), reveal more interesting behavior. By decreasing ν , the energy

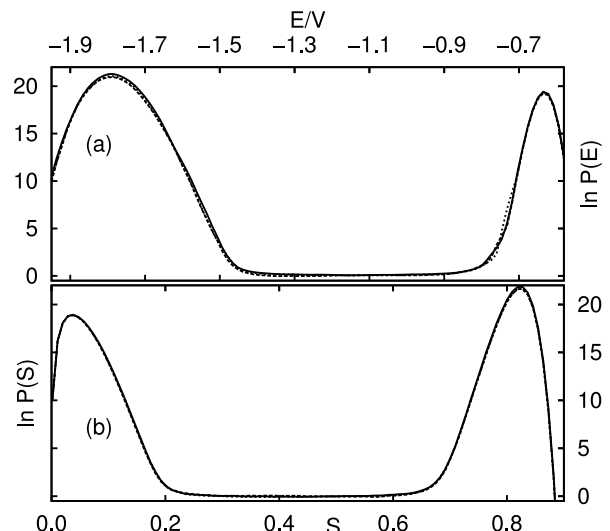


FIG. 6: Order parameter distributions of Eq.(4) with $p = 10$ and $\nu = 0$, obtained using box dimensions $L = 10$ and $D = 30$. Shown are the logarithm of the energy distribution (a), and of the nematic order parameter (b). In each case, three distributions are shown, corresponding to homogeneous and homeotropic enforced anchoring, as well as no enforced anchoring direction. The curves overlap almost perfectly, indicating the absence of any anchoring effects.

difference between the isotropic and the nematic phase becomes smaller. In other words, the transition becomes weaker. The simulations do not rule out that the curves meet when ν becomes sufficiently negative, possibly terminating in a critical point, but clearly additional efforts are required to resolve this. All that matters for the present work, however, is the fact that Fig. 5(b) reveals a large coexistence region, over a substantial range of ν values. This confirms our expectation that, by using $p = 10$ in Eq.(4), the first-order nature of the transition is enhanced significantly. This makes the model ideal to study anchoring effects, with which we proceed next.

C. Anchoring effects for $\nu = 0$

As a benchmark, we consider Eq.(4) with $\nu = 0$, using the newly proposed method. Note that, for $\nu = 0$, the model is spatially isotropic, and so we do not expect to see any anchoring effects. We MC simulate Eq.(4) as before, with the constraint of Eq.(3) explicitly included. Two anchoring conditions are considered: homogeneous and homeotropic. Recall that the anchoring is set via θ_t in Eq.(3). For the threshold angle, we use $\delta = 0.75$ degrees. In addition to $P(E)$, we also measure $P(S)$, with S the nematic order parameter defined in Section II A. For completeness, we mention that our simulations are performed using a bias on the nematic order parameter S , see details in Ref. 19.

The resulting energy distributions are given in

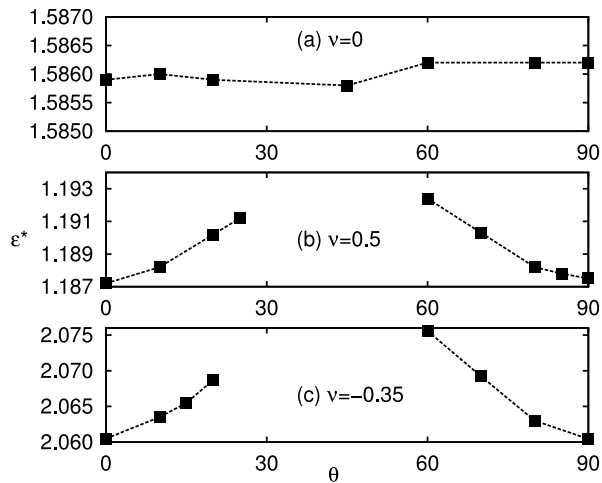


FIG. 7: Transition inverse temperature ϵ^* versus anchoring angle θ for Eq.(4) with $p = 10$ and three values of ν as indicated. Closed symbols are actual simulation data; lines serve to guide the eye. The data were obtained using box dimensions $L = 15$ and $D = 40$. Note the much finer scale in (a) compared to (b) and (c).

Fig. 6(a), which actually shows three distributions. Shown are the two distributions obtained using the new method, corresponding to homogeneous and homeotropic anchoring, as well as the distribution obtained without any enforced anchoring. The striking feature is that the curves overlap almost perfectly. This result is crucial because it demonstrates the consistency of the method. First of all, the insensitivity of the peak positions with respect to the enforced anchoring, confirms that *bulk* properties are *not* affected by the constraint. In addition, we find that the barrier ΔF , defined in Fig. 2(b), also does not depend on the anchoring condition. In other words, the interfacial tension is independent of the tilt angle, which is precisely what one expects for an isotropic potential. Additional confirmation of the consistency of the new method is provided in Fig. 6(b), which shows the corresponding distributions $\ln P(S)$ of the nematic order parameter. Again, the curves overlap almost perfectly. Note also that, for the interfacial tension, it does not matter whether one reads-off the barrier height in $\ln P(E)$ or $\ln P(S)$. As Fig. 6 shows, the barriers are nearly equal (the slight variation gives an indication of the statistical uncertainty).

We have repeated the above analysis using larger lattices, considering also tilt angles between 0 and 90 degrees. Shown in Fig. 7(a) is the transition inverse temperature ϵ^* versus θ . As expected, for the spatially isotropic case, ϵ^* is insensitive to θ , and we obtain $\epsilon^* = 1.5860 \pm 0.0005$. Shown in Fig. 8 is the angle dependent interfacial tension $\gamma(\theta)$, as extracted from the barrier ΔF in $\ln P(S)$ and using Eq.(2). Here, ΔF was taken to be the average height of the peaks, measured with respect to the flat region. As expected, the inter-

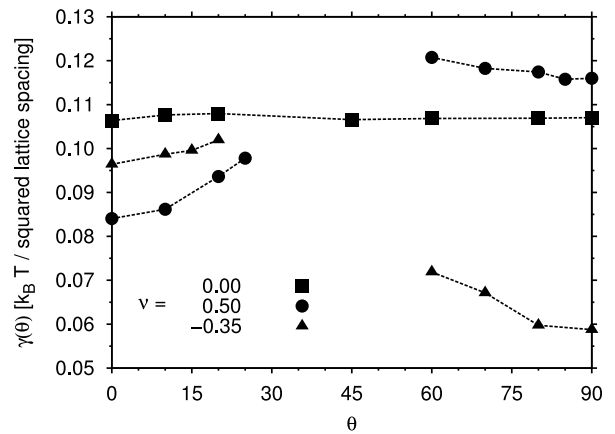


FIG. 8: Angle dependent interfacial tension $\gamma(\theta)$ of Eq.(4) using $p = 10$ and three values of ν as indicated. Closed symbols are actual simulation data; lines serve to guide the eye. The data were obtained using box dimensions $L = 15$ and $D = 40$.

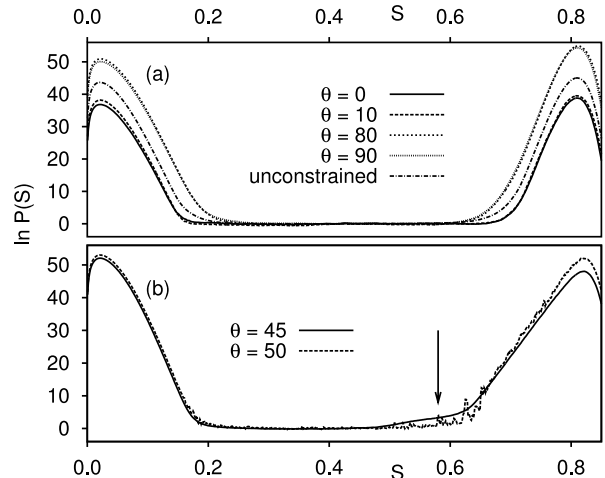


FIG. 9: Logarithm of the nematic order parameter distribution $P(S)$, at coexistence, of Eq.(4) with $p = 10$ and $\nu = 0.5$. Shown is $\ln P(S)$ for various imposed anchoring angles θ , with θ the angle between the nematic director and the plane of the IN interface. The distributions were obtained using box dimensions $L = 15$ and $D = 40$.

facial tension does not display any pronounced θ dependence (the variation stays below 2%). For $\nu = 0$, we thus find $\gamma = 0.108 \pm 0.002 k_B T$ per squared lattice spacing, independent of the tilt angle.

D. Anchoring effects for $\nu = 0.5$

Having verified that the spatially isotropic case $\nu = 0$ does not reveal any anchoring effects, we now consider Eq.(4) using $\nu = 0.5$. In this case, the model becomes anisotropic, and the tilt angle of the nematic phase with respect to the IN interface should become a relevant pa-

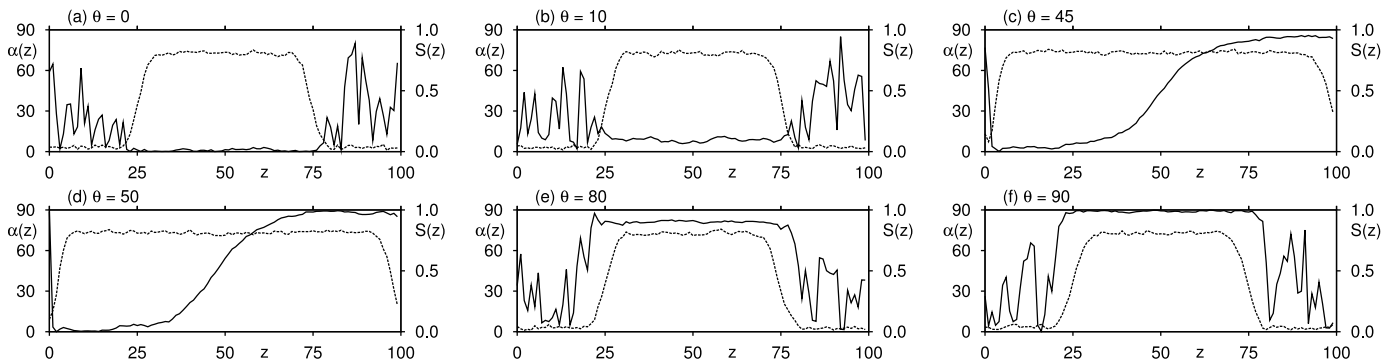


FIG. 10: Profiles $S(z)$ (dashed curves) and $\alpha(z)$ (solid curves) of Eq.(4) with $p = 10$ and $\nu = 0.5$, for various imposed tilt angles θ . The profiles were obtained at the transition inverse temperature ϵ^* , overall nematic order parameter $S = 0.4$, and box dimensions $L = 40$ and $D = 100$.

parameter. For a number of tilt angles, we have measured the order parameter distribution $\ln P(S)$ at coexistence; recall that the tilt angle is set via the constraint of Eq.(3). Typical distributions are plotted in Fig. 9. Shown in (a) are distributions for tilt angles close to homogeneous and homeotropic anchoring; shown in (b) are distributions for two “in-between” tilt angles. Also shown in (a) is the “unconstrained” distribution, which one obtains without imposing the constraint of Eq.(3). For tilt angles that are close to $\theta = 0$ or $\theta = 90$, the distributions behave as expected: they are bimodal, and also exhibit a pronounced flat region between the peaks. In addition, we observe that the barrier height, defined in Fig. 2, depends profoundly on the imposed tilt angle. Since the barrier is related to the interfacial tension, via Eq.(2), we can already see that anchoring effects are present. Interestingly, for the “in-between” tilt angles, bimodal distributions can also be identified, but the region between the peaks is not quite flat, see the arrow in Fig. 9(b). This suggests that, for these “in-between” angles, the constraint does not quite produce the IN coexistence scenario of Fig. 3, but rather something else.

To verify what is going on, we have generated a number of snapshots, at *fixed* nematic order parameter $S = 0.4$. For all distributions in Fig. 9, this value is well between the peak positions. The snapshots are generated at the transition inverse temperature ϵ^* using MC simulation. After equilibration, we collect the profiles $S(z)$ and $\alpha(z)$. Here, $S(z)$ is the nematic order parameter in the z -th $L \times L$ slab perpendicular to the elongated \hat{z} -direction, and $\alpha(z)$ the angle between the director in that slab and the xy -plane. The profiles are shown in Fig. 10, for the same tilt angles as studied in Fig. 9. For $\theta = 0, 10, 80, 90$ degrees, the profile $S(z)$ strikingly confirms IN phase coexistence. We can clearly identify one region where $S(z)$ is close to zero, corresponding to the isotropic phase, and another region where $S(z)$ is closer to unity, corresponding to the nematic phase. Moreover, in the nematic phase, $\alpha(z)$ is roughly constant, and the plateau value closely follows the imposed anchoring angle θ . In other

words, the constraint has the expected effect, namely to force the nematic phase to assume a specified tilt angle. Of course, in the isotropic phase, there is no preferred direction, and $\alpha(z)$ fluctuates randomly; one can show that the average should converge to $90(\pi - 2)/\pi \approx 32.7$ degrees. In contrast, for $\theta = 45, 50$ degrees, the scenario is completely different. Here, $S(z)$ is roughly constant at $S \approx 0.8$, implying a single nematic phase along the entire \hat{z} -direction. In addition, from the corresponding $\alpha(z)$, we see that the nematic is twisted: starting at $z = 0$, $\alpha(z)$ rotates smoothly from 0 to 90 degrees, abruptly dropping back to 0 again as one passes through the periodic boundary at $z = 100$. Clearly, this configuration does not reflect IN coexistence at all, but rather a twisted nematic phase with a surface defect.

In light of Fig. 10, it is clear that the free energy barrier for “in-between” tilt angles does not reflect the interfacial tension, and consequently Eq.(2) does not apply. For angles that are close to homogeneous and homeotropic anchoring, however, the IN scenario of Fig. 3 is confirmed. Therefore, for these angles, we may use Eq.(2) to obtain the angle dependent interfacial tension $\gamma(\theta)$. The result is shown in Fig. 8, which reveals several trends. First of all, in contrast to $\nu = 0$, we now observe a profound variation of $\gamma(\theta)$ with the imposed tilt angle. The interfacial tension is smallest at $\theta = 0$, corresponding to homogeneous anchoring. We therefore expect unconstrained simulations, whereby θ is not imposed but freely fluctuating, to mostly exhibit homogeneous anchoring. However, the data of Fig. 8 also suggest the presence of a shallow minimum at $\theta = 90$, which corresponds to homeotropic anchoring. In other words, for $\nu = 0.5$, homeotropic anchoring appears to be metastable. Since the difference in interfacial tension between homogeneous and homeotropic anchoring is small, it is not *a-priori* clear which anchoring condition will actually prevail in an unconstrained simulation.

We have therefore performed a number of unconstrained simulations, i.e. without Eq.(3), and measured the coexistence distribution $\ln P(S)$. In addition, for each

simulation, we also recorded the n_z component of the director \vec{n} as a function of S . In some cases, we found that the system selects $\theta = 0$, in which case n_z drops to zero once nematic order sets in, but quite often also $\theta = 90$ is selected, in which case n_z becomes close to unity. More precisely, using lattice dimensions $L = 15$ and $D = 40$, we performed 90 unconstrained simulations and found that metastable homeotropic anchoring ($\theta = 90$) was selected 27 times, i.e. in 30% of the cases. This finding is important because it shows that the order parameter distribution of the unconstrained simulation actually reflects a “weighted average” of both stable and metastable anchoring. This feature is illustrated in Fig. 9(a), which also includes $\ln P(S)$ of the unconstrained simulation. As the figure shows, the free energy barrier of the unconstrained simulation is somewhere “in-between” homogeneous and homeotropic anchoring.

Another important finding is that the unconstrained simulations reveal only stable anchoring ($\theta = 0$), and metastable anchoring ($\theta = 90$), while no other anchoring angles were observed. This result is consistent with $\gamma(\theta)$ of Fig. 8, which indeed features just two minima. In other words, all “in-between” tilt angles are unstable. Systems in which the anchoring is held artificially fixed at such unstable angles, for example via the constraint of Eq.(3), will experience an additional strain. For highly unstable tilt angles, the strain is so strong, that it becomes favorable for the system to break-up the IN interfaces altogether, and form a twisted nematic. This is precisely the effect we observed for $\theta = 45, 50$ in Fig. 10. However, also for tilt angles close to the stable and metastable angle, we noticed that the strain manifests itself. In this case, a small shift in the transition inverse temperature ϵ^* can be detected. The effect is illustrated in Fig. 7(b), which shows ϵ^* as a function of the imposed tilt angle θ . For unstable tilt angles, ϵ^* is systematically larger compared to the stable and metastable angles. Of course, for the stable and metastable angles, which are the experimentally relevant cases, one finds the same transition temperature again. Note also Fig. 7(a), which shows that the effect for the spatially isotropic potential $\nu = 0$ does not occur, as expected.

E. Anchoring effects for $\nu = -0.35$

For completeness, we also performed a number of simulations using a negative value of ν in Eq.(4), namely $\nu = -0.35$. Recall that for negative values, the side-side arrangement of Fig. 4 becomes energetically more favorable. Compared to $\nu = 0.5$, one might intuitively expect that this reverses the stable and metastable anchoring angles. The angle dependent interfacial tension indeed confirms this, see Fig. 8. We now observe that homeotropic anchoring yields the lowest interfacial tension, i.e. is stable, while homogeneous anchoring appears to be metastable. In agreement with $\nu = 0.5$, we again measure a shift in ϵ^* when unstable anchoring angles are

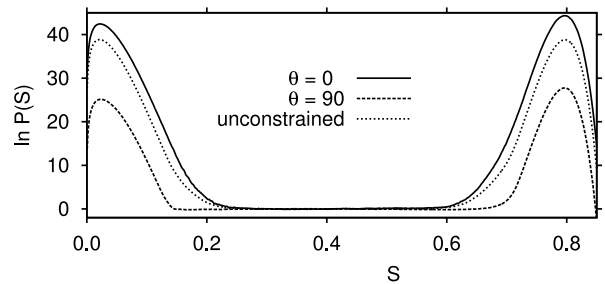


FIG. 11: Coexistence distributions $\ln P(S)$ of Eq.(4), with $p = 10$ and $\nu = -0.35$, using box dimensions $L = 15$ and $D = 40$. Shown are distributions for imposed tilt angles $\theta = 0, 90$ degrees, as well as the unconstrained distribution that one obtains when the tilt angle is allowed to freely fluctuate.

imposed, see Fig. 7(c). Interestingly, even though for $\nu = -0.35$ homeotropic anchoring yields the lowest interfacial tension, we observed that *unconstrained* simulations have difficulty “finding” this configuration. During a series of 95 unconstrained simulation runs, homeotropic anchoring was selected only 35 times, i.e. in 37% of the cases. In other words, the interfacial tension extracted from $\ln P(S)$ in the unconstrained simulation, rather reflects the metastable anchoring condition, see Fig. 11. The figure clearly shows that homeotropic anchoring ($\theta = 90$) yields the lowest free energy barrier, while the barrier in the unconstrained distribution is significantly higher (and, in fact, rather closely resembles homogeneous anchoring). From a computational point of view, the result of Fig. 11 is important because it shows that simulations do not generally find the optimal anchoring angle by themselves, even in a relatively simple lattice model.

IV. RESULTS: SOFT RODS

Next, we investigate anchoring effects in an *off-lattice* fluid of soft rods. The rods are modeled as spherocylinders, of length l and width w . In this section, we set $l/w = 10$, and w will be the unit of length. The rods interact via a repulsive pair potential, whereby rod overlap is penalized with an energy cost of $2k_B T$. For more details about the model, the reader is referred to previous work [18, 19]. The rods are simulated in the grand-canonical ensemble, i.e. at constant temperature T , chemical potential μ , and system volume V , while the number of rods in the system fluctuates. Again, we use an elongated simulation box $V = L \times L \times D$, with periodic boundary conditions. The simulations are performed using standard insertion/deletion moves [34], and the distribution $\ln P(S)$ is recorded, defined as the probability to observe the nematic order parameter S , at the specified tilt angle θ . As before, θ is imposed using the constraint of Eq.(3). For soft rods, we noticed that a substantially larger threshold angle was needed to maintain

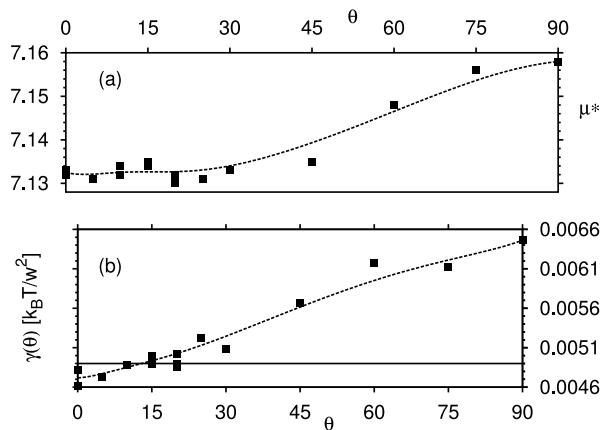


FIG. 12: Anchoring properties of soft rods at the IN transition. Shown in (a) is the coexistence chemical potential μ^* versus θ ; in (b) the angle dependent interfacial tension $\gamma(\theta)$ versus θ . Closed squares are raw simulation data; the curves serve to guide the eye. The horizontal line in (b) marks the interfacial tension of an *unconstrained* simulation, taken from previous work [19]. The simulations were performed using box dimensions $L = 35$ and $D = 105$.

efficiency. Here, we used $\delta = 2.5$ degrees. Whereas in the thermotropic liquid crystal of Eq.(4) phase coexistence is achieved by tuning the inverse temperature ϵ , here that role is played by the chemical potential μ . At the coexistence chemical potential μ^* , $\ln P(S)$ becomes bimodal: coexistence properties and interfacial tensions may then be extracted from the peak positions and heights, as in Fig. 2.

The results of the soft rod simulations are summarized in Fig. 12. Compared to the lattice simulations of Eq.(4), the data reveal significant scatter. This indicates that soft rod simulations are demanding, and already close to the limit of what is currently tractable. Nevertheless, a number of trends emerge. According to Fig. 12(b), $\gamma(\theta)$ increases monotonically with θ , with the minimum occurring at $\theta = 0$. In other words, soft rods favor homogeneous anchoring, and the presence of metastable angles is unlikely. The data also show that the anchoring angle is a remarkably “soft” degree of freedom: the free energy cost of tilting the nematic director away from the IN interface is small. This is apparent from the coexistence chemical potential, see Fig. 12(a). Note that Fig. 12(a) is the “analogue” of Fig. 7 for the lattice model of Eq.(4). For the lattice model, the coexistence inverse temperature increases profoundly away from the stable and metastable angles. This increase is a manifestation of the strain introduced into the system when *unstable* anchoring angles are imposed. In contrast, for soft rods, the coexistence chemical potential remains nearly constant over a wide range; only when $\theta > 30$ or so, does μ^* begin to exhibit a pronounced θ dependence. For soft rods, the anchoring angle can thus be varied around the stable direction over a fairly large range, without intro-

ducing excessive strain into the system. This result is important for *unconstrained* simulations, where the anchoring angle is allowed to fluctuate freely. It is unlikely that such simulations would always reveal homogeneous anchoring. Rather, we expect a range of anchoring angles $0 < \theta < 30$ to be present. The horizontal line in Fig. 12(b) marks the interfacial tension obtained during an *unconstrained* simulation of soft rods [19], and indeed confirms this expectation. Even though the lowest interfacial tension is obtained at $\theta = 0$, the unconstrained simulation slightly exceeds this value. Instead, it rather reflects the average of $\gamma(\theta)$ over the range $0 < \theta < 30$ degrees. Additional confirmation is obtained from simulation snapshots of *unconstrained* simulations, which reveal substantial fluctuations of the anchoring angle around the homogeneous direction.

V. SUMMARY AND OUTLOOK

In this paper, an alternative simulation approach to study anchoring effects at the IN interface in liquid crystals was described. In particular, we focused on the angle dependent interfacial tension $\gamma(\theta)$, with θ the anchoring or tilt angle. The proposed method is based on recent innovations [18, 19] where the order parameter distribution is used to extract interfacial properties. The new twist has been to introduce a constraint into the Hamiltonian, see Eq.(3), which forces the nematic director to maintain a specified angle with respect to the xy -plane. The idea is that, by using a simulation box that is elongated in the z -direction, IN interfaces will form in the xy -plane as well. The constraint then allows the anchoring angle θ to be fixed to some value of interest.

At the same time, a new liquid crystal model was introduced. The model is defined on a lattice and exhibits a strong first-order IN transition. In addition, the preferred anchoring (homogeneous, homeotropic, or neutral) can be tuned by means of a single parameter. Compared to more elaborate *off-lattice* models, such as rods or platelets, the lattice variant is considerably easier to simulate. In particular, equilibration is less problematic, and high-quality data are readily generated. Precisely this property was exploited to obtain $\gamma(\theta)$ for the lattice model, using the new method. Indeed, when anchoring effects are “switched-off”, by setting $\nu = 0$ in Eq.(5), $\gamma(\theta)$ becomes constant. In contrast, when $\nu \neq 0$, a pronounced θ dependence is revealed. For these cases, only homogeneous and homeotropic anchoring were seen to be relevant. More precisely, for $\nu > 0$, homogeneous anchoring is stable, and homeotropic anchoring metastable. For $\nu < 0$, the trend is reversed. In other words, the preferred anchoring depends sensitively on the details of the interactions. Our results have also shown that, when unstable anchoring angles are imposed, the new method must be used with some care. In those cases, the simulations do not reveal IN coexistence, but rather a twisted nematic phase. Fortunately, when this happens, the method gives

a clear warning, in the form of a shift in the coexistence temperature. A somewhat surprising finding was that, even for the simple lattice model, simulations do not generally find the “optimal” anchoring angle by themselves. Instead, when the nematic director is allowed to fluctuate freely, both stable and metastable anchoring are typically revealed.

We have also applied the new method to obtain $\gamma(\theta)$ for a fluid of soft rods. For soft rods, anchoring effects could also be identified, albeit that the data are significantly less accurate. The simulations reveal homogeneous anchoring to be stable, a finding which is consistent with most theoretical studies of hard rods. Interestingly, for soft rods, no metastable anchoring angle could be detected, which makes this model qualitatively very different from the lattice model of Eq.(4). It confirms, once again, that anchoring effects are extremely sensitive to the particle interactions.

For the future, investigations of the capillary wave spectrum for the lattice model of Eq.(4) are planned. As mentioned in the Introduction, the spectrum is qualitatively affected by the anchoring condition [5, 6, 7]. Since, in Eq.(4), the anchoring can be tuned using a single parameter, and since the model is easy to simulate anyhow, such investigations should be worthwhile. A sound understanding of the lattice model may well be a prerequisite before more complicated *off-lattice* simulations are attempted.

Acknowledgments

This work was supported by the *Deutsche Forschungsgemeinschaft* under the SFB-TR6 (project section D3).

-
- [1] L. Onsager, *Ann. N. Y. Acad. Sci.* **51**, 627 (1949).
 [2] B. Jerome, *Phys. Rep.* **54**, 391 (1991).
 [3] J. S. Patel and H. Yokoyama, *Nature* **362**, 525 (1993).
 [4] F. Barmes and D. J. Cleaver, *Phys. Rev. E* **71**, 021705 (2005).
 [5] N. Akino, F. Schmid, and M. P. Allen, *Phys. Rev. E* **63**, 041706 (2001).
 [6] J. Elgeti and F. Schmid, *Eur. Phys. J. E* **18**, 407 (2005).
 [7] F. Schmid, G. Germano, S. Wolfsheimer, and T. Schilling, *Fluctuating interfaces in liquid crystals* (2007).
 [8] S. Wolfsheimer, C. Tanase, K. Shundyak, R. van Roij, and T. Schilling, *Phys. Rev. E* **73**, 061703 (2006).
 [9] Z. Y. Chen and J. Noolandi, *Phys. Rev. A* **45**, 2389 (1992).
 [10] E. Velasco, L. Mederos, and D. E. Sullivan, *Phys. Rev. E* **66**, 021708 (2002).
 [11] W. E. McMullen, *Phys. Rev. A* **38**, 6384 (1988).
 [12] B. G. Moore and W. E. McMullen, *Phys. Rev. A* **42**, 6042 (1990).
 [13] D. L. Koch and O. G. Harlen, *Macromolecules* **32**, 219 (1999).
 [14] K. Shundyak and R. van Roij, *J. Phys.: Condens. Matter* **13**, 4789 (2001).
 [15] M. P. Allen, *Chem. Phys. Lett.* **331**, 513 (2000).
 [16] A. J. McDonald, M. P. Allen, and F. Schmid, *Phys. Rev. E* **63**, 010701(R) (2000).
 [17] P. A. Lebowitz and G. Lasher, *Phys. Rev. A* **6**, 426 (1972).
 [18] R. L. C. Vink and T. Schilling, *Phys. Rev. E* **71**, 051716 (2005).
 [19] R. L. C. Vink, S. Wolfsheimer, and T. Schilling, *J. Chem. Phys.* **123**, 074901 (2005).
 [20] K. Binder and D. P. Landau, *Phys. Rev. B* **30**, 1477 (1984).
 [21] K. Binder, *Phys. Rev. A* **25**, 1699 (1982).
 [22] B. Grossmann and M. L. Laursen, *Nucl. Phys. B* **408**, 637 (1993).
 [23] D. van der Beek, H. Reich, P. van der Schoot, M. Dijkstra, T. Schilling, R. Vink, M. Schmidt, R. van Roij, and H. Lekkerkerker, *Phys. Rev. Lett.* **97**, 087801 (2006).
 [24] P. Virnau and M. Müller, *J. Chem. Phys.* **120**, 10925 (2004).
 [25] Z. Zhang, O. G. Mouritsen, and M. J. Zuckermann, *Phys. Rev. Lett.* **69**, 2803 (1992).
 [26] A. C. D. van Enter and S. B. Shlosman, *Phys. Rev. Lett.* **89**, 285702 (2002).
 [27] E. Domany, M. Schick, and R. H. Swendsen, *Phys. Rev. Lett.* **52**, 1535 (1984).
 [28] H. W. J. Blöte, W. Guo, and H. J. Hilhorst, *Phys. Rev. Lett.* **88**, 047203 (2002).
 [29] A. C. D. van Enter, S. Romano, and V. A. Zagrebnov, *J. Phys. A* **39**, L439 (2006).
 [30] R. L. C. Vink, *Phys. Rev. Lett.* **98**, 217801 (2007).
 [31] N. V. Priezjev, G. Skačej, R. A. Pelcovits, and S. Žumer, *Phys. Rev. E* **68**, 041709 (2003).
 [32] A. M. Ferrenberg and R. H. Swendsen, *Phys. Rev. Lett.* **61**, 2635 (1988).
 [33] M. E. J. Newman and G. T. Barkema, *Monte Carlo Methods in Statistical Physics* (Clarendon Press, Oxford, 1999).
 [34] D. Frenkel and B. Smit, *Understanding Molecular Simulation* (Academic Press, San Diego, 2001).